Infrared photoconductivity of nanocrystal-sensitized polymers

Peter Fonteijn

Top Master Nanoscience
Zernike Institute for Advanced Materials
University of Groningen

Supervisor: Dr. Maria Antonietta Loi

University of Groningen
Zernike Institute
for Advanced Materials

Copyright © Peter Fonteijn, June 2007

Infrared photoconductivity of nanocrystal-sensitized polymers

Peter Fonteijn

Top Master Nanoscience
Zernike Institute for Advanced Materials
University of Groningen

June 2007

The detection of infrared light is an important research area, interesting for many applications like environmental monitoring, thermal imaging, night vision, fibre-optic telecommunication systems and imaging of biomedical assays. Nature provides some crystalline materials with a band gap energy suitable for absorption of infrared light. These materials impose however requirements on fabrication. In search for better materials, one ended at organic conjugated polymers. Polymers provide low costs, physical flexibility and large area coverage together with easy chemical synthesis and simple processing. Until today however no polymers have been developed with a band gap energy equal to that needed for most of the practical infrared photoconduction applications.
A new approach combines the low band gap energy of the traditional semiconductors with the easy to process polymers. Semiconductor nanocrystals are used because of the tunability of their absorption peak due to the quantum size effect. These nanocrystals sensitize the polymers in order to observe photoconductivity into the infrared region of the electromagnetic spectrum. This essay reviews recent results on nanocrystal–polymer composites developed for showing the photoconductive behaviour in the infrared region. It also explains about the photoconductive effect, the phenomenon of sensitization and nanocrystal tunability.

Contents

1 – Introduction: the first steps to light detection

Scientific understanding begins with observation. Optical phenomena and imaging have been of interest for ages. Euclid was one of the first to study reflection and refraction. Scientific knowledge developed and optical instruments containing lenses were designed. Later on also capturing of images, in the sense of photography, became seen as very interesting. Eventually detection of light became an important research area.[1]

The first significant discovery was made in 1839. Edmund Becquerel, a French experimental physicist, noticed a current on illuminating platinum electrodes.[2, 3] The platinum electrodes, as parts of an electrolytic cell, where covered with silver bromide or silver chloride and immersed in an aqueous solution. Strictly speaking Becquerel observed a photochemical effect. Nevertheless, he was the first who described the conversion of light into electrical power. Therefore the discovery of the photovoltaic effect is commonly ascribed to Becquerel.[4]

In 1873 Willoughby Smith discovered the photoconductive effect when he experimented with selenium as an insulator for submarine cables.[5] Three years later W.G. Adams and R.E. Day made another report on photoconductivity working on selenium.[6] These discoveries were a starting point for a large field of investigations for several decades.[7] Most of the work was of doubtful quality, but at least the first step in detection of light, getting a measurable signal on illumination, was made.

2 – The photoconductive effect

2.1 Defining the photoconductive effect

Photoconductivity is a process that can occur in semiconductor materials. In a semiconductor the electron energy levels are arranged in energy bands (valence band and conduction band) separated by a region in energy for which no electron levels exist. This forbidden region is known as the energy gap or band gap.[8]

In an intrinsic semiconductor at room temperature some electrons sitting at the valence band edge have enough thermal energy to cross the band gap. They will occupy an energy level in the conduction band while leaving a hole behind in the valence band, thus generating free carriers (Fig. 1a). When a voltage is applied to two opposite faces of the semiconductor a small current flows. This current, called the dark current, is due to these small numbers of electrons and holes.[9, 10]

When the semiconductor is illuminated with light, energy from the incident photons can be transferred to valence band electrons. If the energy of the incident photons is large enough, these electrons can cross the band gap and occupy energy levels in the conduction band. In this way the free charge carrier density is increased (Fig 1b). If the same voltage is applied across the semiconductor a larger current will flow, called the light current. So by illuminating the semiconductor a change in conductivity can be observed, known as the photoconductive effect.[10, 11]

The frequency range of light that will induce the photoconductive effect depends on the size of the band gap. The photon energy has to be at least equal to the band gap energy.[10] From the definition of the energy of a photon it can be seen that the maximal wavelength allowed to induce the photoconductive effect is

$$\lambda_{\max} = \frac{hc}{E_g}, \qquad (1)$$

in which E_g is the band gap energy and hc the product of Planck's constant with the speed of light.

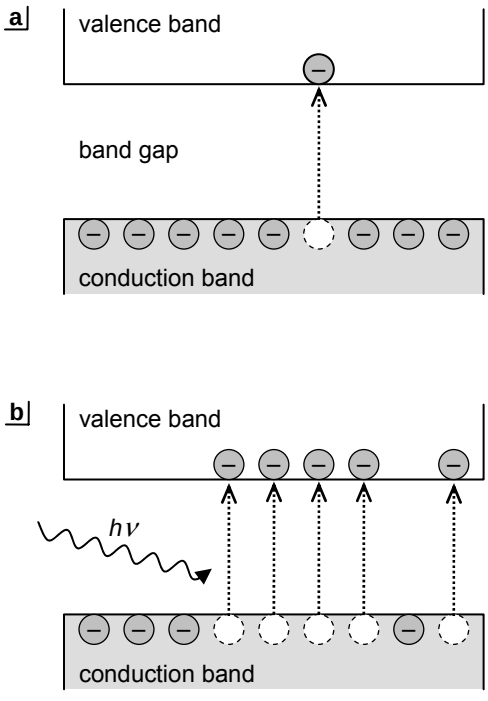

Figure 1 – The photoconductive effect: a change of conductivity on absorption of electromagnetic waves. a) Generation of free charge carriers by thermal energy giving rise to a small dark current.
b) Generation of many free charge carriers on absorption of light giving an increase in conductivity, known as the photoconductive effect.

2.2 The photoconductive effect: a sequence of steps

The photoconductive effect can be split in a sequence of steps.[12-14] First the semiconductor absorbs the illuminating light. As describe above the energy of the incident electromagnetic wave is used to promote an electron from the valence band to the conduction band. The opposite charges of electron and hole however are still Coulombically attracted to each other. Therefore they are considered as a single species called an exciton, a bound electron-hole pair (Fig 2a). Depending on the nature and the dielectric constant of the semiconductor material the exciton is tightly bound (Frenkel exciton) or weakly bound (Mott-Wannier exciton).[8] Because of the binding energy of the exciton, the exciton energy levels lie lower in energy than the conduction band energy levels,[8, 13] effectively lowering the band gap. Therefore light with a wavelength slightly above the maximum wavelength is usually already capable of promoting an electron to higher energy (see equation 1).

In the next step the exciton is dissociated into free charge carriers. For this to occur, the Coulomb binding energy of the bound electron-hole pair has to be overcome. In some cases thermal energy alone is enough, in other cases an electric field assists the separation of charges.[12-14] If no electric field is applied the free carriers will randomly diffuse which results in zero current. To get a measurable current a voltage has to be applied, generating an electric field across the semiconductor. Both electrons and holes will drift towards the electrodes due to the electric field (Fig 2b). This drift in the end is the current that can be measured.

During the photoconduction process recombination can always occur (Fig 2c). The exciton for example will not exist forever. Upon absorption of light, the exciton can decay back to its ground state. In this process the electron drops back into the hole and the exciton is lost (exciton recombination).[8] Another recombination process can occur after the second step of generating free carriers. Diffusion can bring two opposite charges back together and due to the Coulomb attractive forces an exciton can be reformed (bimolecular recombination).[13, 14] This exciton can separate again in free charges or undergo exciton recombination.

Another way of loosing free charge carriers is due to traps.[11-13] Any semiconductor will contain impurities, defects or imperfections, which has their own energy levels. Some of these levels will be situated inside the band gap and are empty energy levels. Both shallow traps and deep traps are usually available. Free charge carriers move around in the semiconductor. When an electron or hole encounters a trap it can lower its energy by occupying this trap energy level (Fig 2d). However, to leave a trap and return to the conduction band or valence band will costs energy again. The amount of energy needed depends on the type of trap (deep trap: large amount of energy, shallow trap: less energy). If this energy is not available the charge carrier is immobilized (trapped) and effectively removed from the set of free charge carriers. Traps therefore have a direct influence on the conductivity.[13, 14]

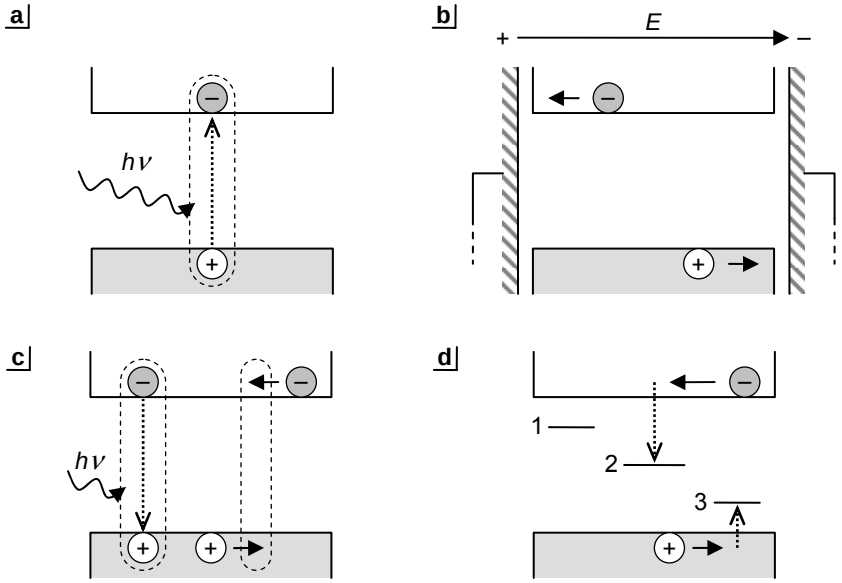

Figure 2 – Different events taking place during the photoconduction process. a) Formation of an exciton, a bound electron-hole pair, on absorption of light. b) Exciton dissociation into free charge carriers followed by drift of the free carriers to the electrodes. c) Two main recombination processes: exciton recombination (left) and bimolecular recombination (right). d) Loss of free charge carriers due to shallow electron traps (1), shallow hole traps (3) and deep traps (2).

2.3 Photocurrent density

In a semiconductor usually both electrons and holes are the free charge carriers that contribute to the conductivity. Conductivity is defined as [8, 9, 11]

$$\sigma = e\,(n\,\mu_e + p\,\mu_h), \tag{2}$$

with n the number of free electrons and p the number of free holes with mobility μ_e and μ_h respectively. Under constant illumination with light, the steady-state concentration of free charge carriers is [12]

$$n = f\,\tau_n \text{ and } p = f\,\tau_p\,. \tag{3}$$

In these equations τ is the average lifetime of the free charge carriers, i.e. the average time before bimolecular recombination takes place, and f the number of photogenerated free charge carriers. The number of photogenerated free charge carriers is given by

$$f = \frac{\phi\, I_A}{L}\,. \tag{4}$$

I_A is the total absorbed intensity of radiation per unit area per unit time and L is the length of the semiconductor material. The quantum efficiency of photogeneration ϕ is the number of free charge carriers generated per number of photons absorbed.

The number of free charge carriers as defined in equation 3 applies on the situation before the semiconductor is connected into a circuit. Measurement of the current though can only be made when a voltage is applied across the material. Application of a voltage however may result in changes in the number of free charge carriers, depending on the nature of the electrodes.[12, 14] With Ohmic contacts the number of free charge carriers is unchanged after connection into the circuit and application of a voltage. As one charge carrier leaves the semiconductor another is immediately injected at the opposite electrode, since there is no energy difference between contact and semiconductor (Fig 3a). In this way the total number of free charge carriers is maintained. With blocking contacts on the other hand, the electrodes do not permit injection of charge carriers into the semiconductor (Fig 3b). In this case the photogenerated charge carriers can only leave the material under influence of an electric field.

Current density is given by Ohm's law [8]

$$J = \sigma\, E \tag{5}$$

and mobility is defined as [9]

$$\mu = \frac{v}{E} = \frac{L}{t_{TR}\,E}\,, \tag{6}$$

in which t_{TR} is the transit time, i.e. the time it takes a free charge carrier to cross the full length of the semiconductor.

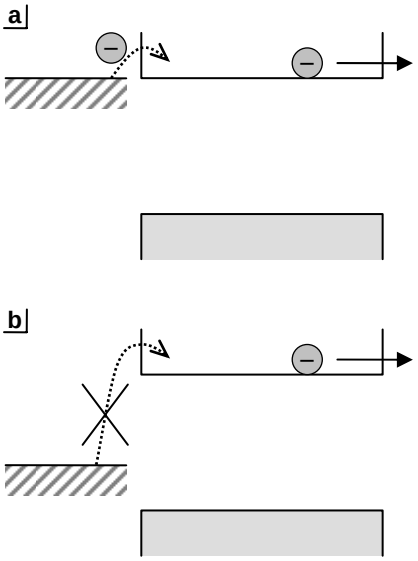

Figure 3 – Ohmic contact versus blocking contact. a) An Ohmic contact electrode gives immediate injection of charge carriers. b) A blocking contact electrode does not permit injection of charge carriers into the semiconductor.

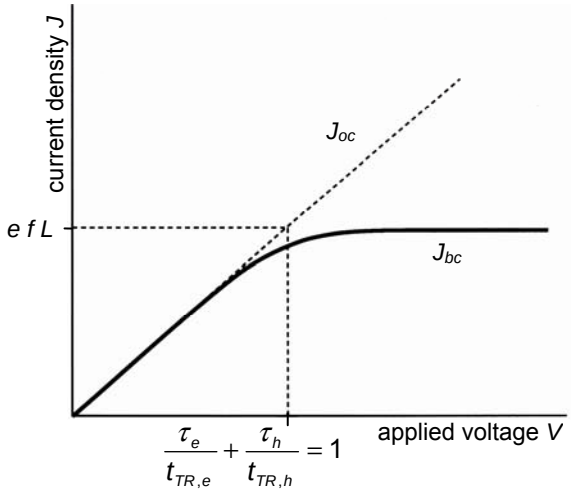

Figure 4 – Steady-state current density. Current density versus applied voltage for Ohmic contact (J_{oc}) and blocking contact (J_{bc}). Note that for constant electric field the voltage is linearly dependent on the field: $V \sim E$. In a photoconduction experiment typically the photocurrent, the dark current subtracted from the light current, as a function of the applied voltage is measured. (adapted from [12])

With Ohmic contacts the steady-state current density therefore becomes [12]

$$J_{oc} = e f L \left(\frac{\tau_e}{t_{TR,e}} + \frac{\tau_h}{t_{TR,h}} \right). \quad (7)$$

With blocking contacts the photogenerated charge carriers can only leave the semiconductor under the influence of an electric field, as described above. For large applied fields the free charge carriers are extracted from the material without recombination taking place, so the (effective) bimolecular recombination time can be considered equal to the transit time.[13] Thus for blocking contacts the steady-state current density is given by [12, 13]

$$J_{bc} = e f L. \quad (8)$$

For lower fields not all free charge carriers are extracted, because bimolecular recombination does occur. So the current density will first follow the behaviour of an Ohmic contact, but will saturate as soon as the transit time becomes smaller than the bimolecular recombination time (Fig. 4).

3 – Infrared light detection

3.1 Semiconductor infrared light detection

The detection of visible light is not the only important research area. Nowadays people focus on the detection of infrared light, which is interesting for many applications. Infrared light is for example critical to environmental monitoring and remote sensing as in the field of astronomy.[15-17] One can also think of thermal imaging, as in infrared cameras, for night vision and night-time surveillance [18-20], fibre-optic telecommunication systems [21] and even imaging of biomedical assays [22, 23].

On the electromagnetic spectrum infrared light lies at a wavelength larger than the visible spectrum (Fig 5). Infrared light has a wavelength of 800 nm (10^{-6} m; near infrared) up to 10^{5} nm (10^{-4} m; far infrared). Telecommunication applications use 1300-1600 nm radiation, thermal imaging 1500 nm and beyond, biological imaging uses transparent tissue windows at 800 nm and 1100 nm, and solar cells and thermal photovoltaics are based on radiation of 800-2000 nm and radiation larger than 1900 nm respectively.[24]

Using equation 1 it can be seen that infrared light in the above range of wavelengths can only induce the photoconductive effect when the band gap energy of the semiconductor is at most 1.5 eV ranging down to 0.01 eV. For most practical applications a band gap energy of about 0.8 eV is necessary (~1500 nm). It is clear that a fairly low band gap is needed to observe the photoconductive effect being induced by infrared light.

Luckily nature provides some crystalline materials with such a low band gap energy (Table 1). Some elemental crystals like silicon and germanium have a low band gap energy. Other low band gap energy crystals are compounds of III-V elements (e.g. InSb, GaAs) or compounds of IV-VI elements (e.g. PbS, SnTe). A lot of research has been performed on these materials to study their infrared photoconductive behaviour. Studies on silicon [25, 26], germanium [27, 28] and gallium arsenide [29, 30] are just some examples of a vast amount of publications that can be found.

Table 1 – Band gap energies for a selection of crystalline materials (adapted from [14])

	band gap energy (eV)	
Crystal	0 K	300 K
Si	1.17	1.11
Ge	0.744	0.66
InSb	0.23	0.17
InAs	0.43	0.36
InP	1.42	1.27
GaAs	1.52	1.43
GaSb	0.81	0.68
PbS	0.286	0.34-0.37
PbSe	0.165	0.27
PbTe	0.190	0.29
SnTe	0.3	0.18

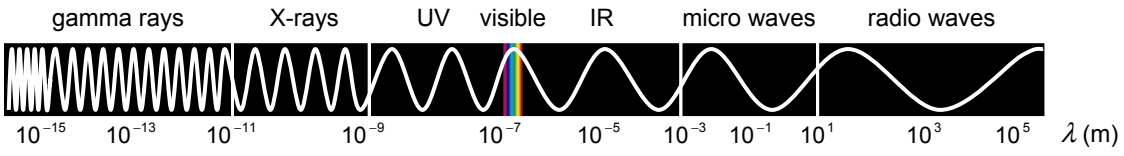

Figure 5 – Electromagnetic spectrum. Schematic of the different regions in the electromagnetic spectrum (not on scale). Infrared light has a wavelength of 800 nm (10^{-6} m; near infrared) up to 10^{5} nm (10^{-4} m; far infrared).

3.2 Organic conjugated polymers

The more or less traditional semiconductor materials impose requirements on fabrication. Therefore the majority of studies are based on lattice-matched, rigid-substrate, epitaxial growth of layered structures of material, mainly by molecular beam epitaxy.[18, 19, 26, 30] Because of the drawbacks of these methods (e.g. the final structures are rigid, it is difficult to obtain large area structures, the costs are relatively high) one started to look for other materials, ending at organic conjugated polymers. In general polymers provide low costs, physical flexibility and large area coverage. They are easily chemically synthesized and are simply processed by methods such as spin or spray coating.[31]
An enormous amount of polymers have been synthesized throughout the years. However, only a few of them have band gap energies below 1.5 eV (Table 2). Until today no organic conjugated polymer has been developed with a band gap energy equal to that needed for most of the practical infrared photoconduction applications (~0.8 eV). Only poly(thieno[3,4-*b*]-thiophene) comes close with a band gap energy of 0.85 eV.[41] From this it is clear that the use of organic conjugated polymers is not a real solution, since these polymers are only sensitive in the very near infrared region. This is obviously not enough for most practical applications. An interesting approach would be to combine the low band gap energy of the traditional semiconductors with the easy to process organic conjugated polymers.

Table 2 – Band gap energies for a selection of recent organic conjugated polymers

band gap energy (eV)	Polymer	Reference
1.4	poly(1,1-dihexyl-3,4-diphenyl-2,5-bis{2-[3,4-ethylenedioxy]thienyl}silole)	[32]
1.28	poly[(α-bithiophene-5,5'-diyl) (5'-(2''-phenyl-1'',3'',4''-oxadiazole-5''-phenylidene))-block-(α-bithiophene(2''-phenyl-1'',3'',4''-oxadiazole-5''-phenylidene)quinodimethane-5, 5'-dily)] (PBTBQ-Oid)	[33]
1.24-1.29	poly(benzo[*c*]thiophene-*N*-2-ethylhexy-4,5-dicarboxylic imide) (EHI-PITN)	[34]
1.1	poly(3,4-ethylenedioxythiophene)-*N*-2'-ethylexyl-4,5-dicarboxylic imide-benzo[*c*]thiophene (PEDOTEHIITN)	[35]
1.10	poly(1,3-bis(2'-[3',4'-ethylenedioxy]thienyl)-benzo[*c*]thiophene-*N*-2''-ethylhexyl-4,5-dicarboximide) P(DEDOT-ITNIm)	[36]
1.03	poly(thieno[3,4-*b*]furan)	[37]
0.94-1.08	poly(thieno[3,4-*b*]thiophene)-poly-(styrenesulfonic acid) (PT34bT-PSS)	[38, 39]
0.92	poly(2-decylthieno[3,4-*b*]thiophene-4,6-diyl)	[40]
0.85	poly(thieno[3,4-*b*]-thiophene)	[41]

4 – Sensitization

All organic conjugated polymers developed so far have a band gap energy such that they are only sensitive to radiation down to the very near infrared. It is possible to extend their sensitivity further into the infrared region to radiation of longer wavelengths by making use of sensitization. In this way it is possible to observe the photoconductive effect in polymeric materials being induced by infrared light.

4.1 Different types of sensitization

In principle two kinds of sensitization are known, called spectral sensitization and chemical sensitization.[42] Spectral sensitization is referred to the appearance of the photoconductive effect in a new region of the electromagnetic spectrum, as is the extension further into the infrared region. Chemical sensitization is referred to only an increase of sensitivity for the incident radiation in a specific region of the spectrum. Both kinds of sensitization usually take place at the same time in a sensitized photoconductor (Fig 6).
Two general types of spectral sensitization are possible,[43] but unfortunately literature is not uniform in terminology. For convenience here the first type is

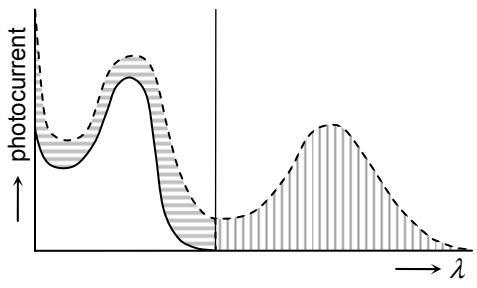

Figure 6 – The two known kinds of sensitization. General photocurrent spectra of a bare photoconductor (solid line) and a sensitized photoconductor (dashed line) showing chemical sensitization (left; horizontal shading) and spectral sensitization (right; vertical shading). Usually both take place at the same time in a sensitized photoconductor.

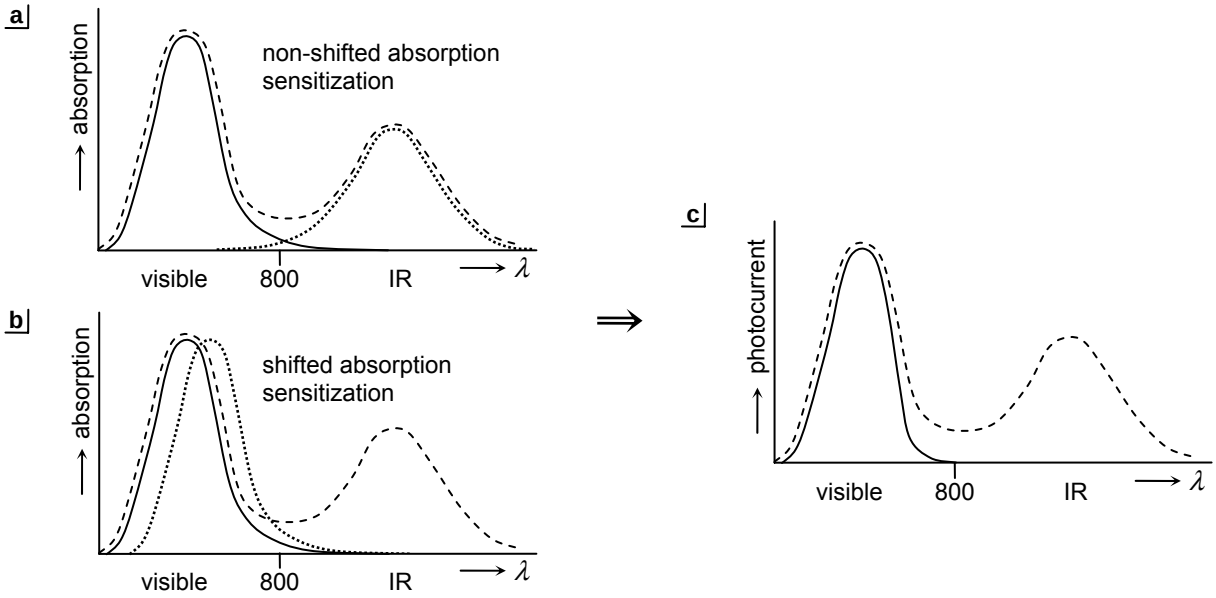

Figure 7 – Two general types of spectral sensitization. a) General absorption spectra of the polymer (solid line), the sensitizer (dotted line) and the sensitized polymer (dashed line) in the case of a non-shifted absorption sensitization. b) General absorption spectra of the polymer (solid line), the sensitizer (dotted line) and the sensitized polymer (dashed line) in the case of a shifted absorption sensitization. c) General photocurrent spectrum of the bare polymer (solid line) and sensitized polymer (dashed line), either due to non-shifted absorption sensitization or shifted absorption sensitization.

called non-shifted absorption sensitization and the second type is called shifted absorption sensitization. The non-shifted absorption sensitization uses a sensitizer with a different band gap energy compared to the polymer. This band gap energy is such that it absorbs radiation in the desired region of the spectrum (Fig 7a). In this way the sensitized polymer will absorb for example infrared light and the photoconductive effect can be observed in the infrared region. The extended sensitivity is directly related to the absorption characteristics of the sensitizer.
The shifted absorption sensitization uses a sensitizer that does not necessarily have a different band gap energy compared to the polymer. Nevertheless the absorption of the sensitized polymer is extended to the desired region of the spectrum (Fig 7b). So also in this case the photoconductive effect can be observed in for example the infrared region. However in this case the extended sensitivity is not directly related to the absorption characteristics of the sensitizer.
With non-shifted absorption sensitization it is the sensitizer that absorbs the illuminating infrared light. As describe above, the energy of the incident electromagnetic wave is used to promote an electron from the valence band to the conduction band, resulting in a Coulombically bound electron-hole pair (an exciton) in the sensitizer. It is the polymeric part however to which the electrodes for charge extraction are connected. So also in the case of sensitization free charges have to be generated somehow in the polymeric material.

4.2 Generation of free charges

There are two ways in which free charges can be generated in the polymeric material: by energy transfer and by charge transfer.[13] In the energy transfer process the excitation energy of the sensitizer is transferred to a molecule with a lower band gap energy. In the case of sensitization of polymers into the infrared this process cannot occur. The polymer has a larger band gap energy than the sensitizer, so the excitation energy of the sensitizer is not enough to promote an electron of the polymer from its valence band to the conduction band (Fig 8a).
In the charge transfer process it is not energy that is transferred, but real charges are transferred to the polymer. With non-shifted absorption sensitization this charge transfer is known as photoinduced charge transfer.[13, 43] It depends on the relative positions of the energy levels whether an electron or a hole is transferred. When the conduction band of the polymer lies below the conduction band of the sensitizer, the excited electron can lower its energy by hopping to the polymer (Fig 8b: left). In this case the sensitizer is called the (electron) donor and the polymer the (electron) acceptor. On the other hand, when the valence band of the sensitizer lies below the valence band of the polymer, the hole

can lower its energy by hopping to the polymer (Fig 8b: right). In this case the sensitizer is called the (electron) acceptor and the polymer the (electron) donor.
Again the photoconductive effect can be split in a sequence of steps as described before.[13, 14] The first step of exciton generation is exactly the same, although it takes place in the sensitizer now. The exciton diffuses through the sensitizer material until it finds the lower energy levels of the polymer. Now the actual charge transfer takes place, resulting in a charge transfer state. In the charge transfer state the electron and hole are in principle still Coulombically bound to each other (Fig 8c). However, when the energy lowering is large enough, the Coulomb binding energy can be overcome and the exciton will be dissociated into free charge carriers. If the energy lowering is not large enough, free charges can be generated either by thermal energy or by assistance of an applied electric field. The free charges are again extracted from the polymer by an applied electric field. Also traps and recombination still play a role. One extra recombination process is however possible: recombination of the Coulombically bound charge transfer state. This process is known as geminate recombination (Fig 8c). The Braun model, a kinetic model for field-assisted dissociation of charge transfer states, describes the theory of the process of photoinduced charge transfer in more detail.[44]
With shifted absorption sensitization free charges are also generated by charge transfer, however in a slightly different way. As explained above the shifted absorption sensitization does not necessarily have a lower band gap energy compared to the polymer. The extended sensitivity to another region of the electromagnetic spectrum is due to direct charge transfer from the sensitizer to the polymer without going to the excited state of the sensitizer molecule.[13, 43] This process is known as charge transfer absorption. If the sensitizer is a strong (electron) donor, it has a low ionization potential or work function, so it is easy to remove an electron from its valence band. In the same way if the polymer is a strong (electron) acceptor, it has a high electron affinity or work function, so it is easy to add an electron to its conduction band. When a strong donor sensitizes a strong acceptor, an electron from the valence band of the sensitizer is promoted to the conduction band of the polymer (Fig 8d).

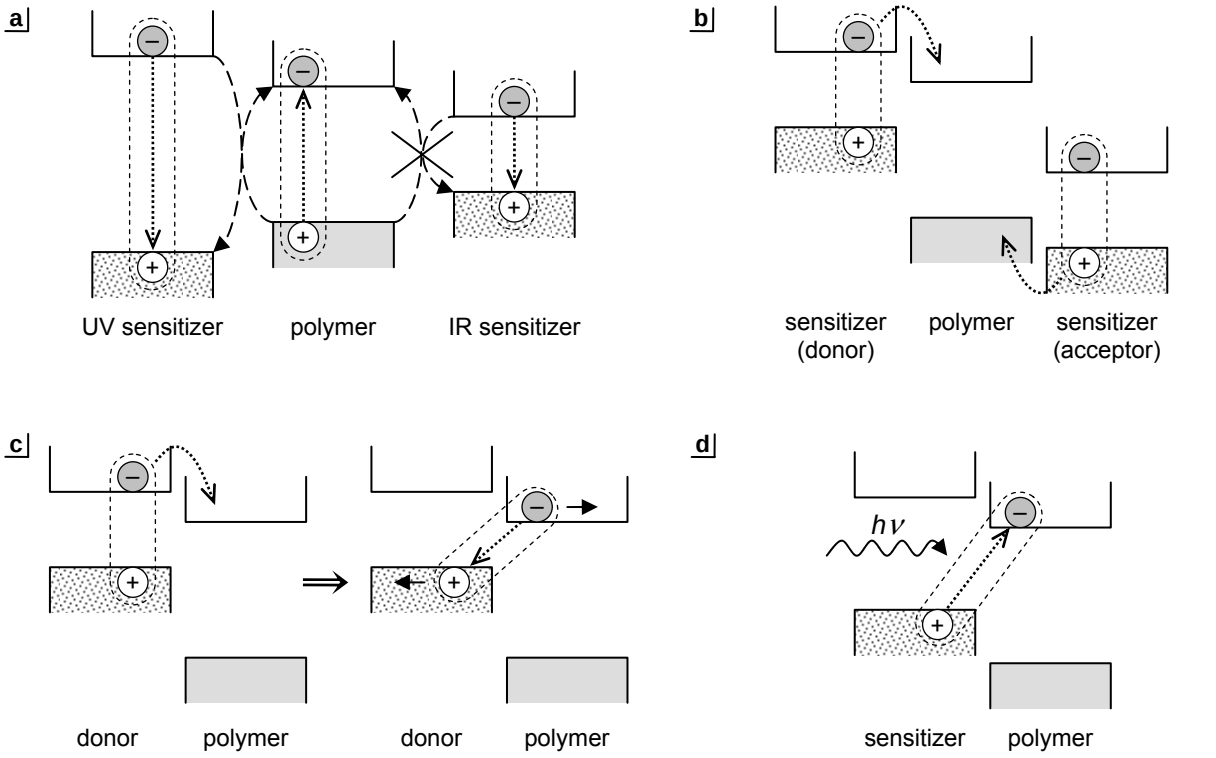

Figure 8 – Different ways of generating free charge carriers in a sensitized polymer. a) Energy transfer process (non-shifted absorption sensitization). The excitation energy of the sensitizer is used to promote an electron of the polymer from the valence band to the conduction band. An infrared sensitizer does not have enough excitation energy for this process to occur. b) Photoinduced charge transfer process (non-shifted absorption sensitization). The sensitizer can either be donor (left) or acceptor (right). c) In the charge transfer state the electron and hole are still Coulombically bound to each other. Arrows indicate dissociation into free charge carriers and geminate recombination respectively. d) Charge transfer absorption process (shifted absorption sensitization). Light absorbed is used for direct charge transfer from the sensitizer to the polymer. The charge transfer complex exciton is formed directly, without going to the excited state of the sensitizer.

Again a charge transfer complex exciton is formed, that can be dissociated into free charge carriers by thermal energy or by assistance of an applied electric field. The conduction band of the polymer lies below the conduction band of the sensitizer. Therefore, the charge transfer absorption transitions require less energy than electronic transitions in the sensitizer or polymer itself. This is way the energy that is absorbed, is extended into the infrared region.

5 – Nanocrystals

Any molecule that is able to shift the sensitivity of a polymer into the infrared region may be used as a sensitizer. Since some of the traditional semiconductors have a low band energy (see Table 1), one thought it would be an interesting approach to combine these semiconductors with the easy to process organic conjugated polymers. Moreover, the combination of traditional electron conducting semiconductors with hole conducting polymers in a single composite provides effective charge separation and transport.[45] It is however not possible to use the semiconductors in the bulk crystalline form, because this will annul the easy processing property. This is why one focussed on nanocrystals.

5.1 Nanocrystals and the quantum confinement effect

A nanocrystal (Fig 9a) is a solid confined in three orthogonal directions, creating effectively a zero-dimensional structure.[8] Confinement means in this case that the size of the solid is of the nanometre scale in all directions. The electrical and optical properties of a solid usually do not depend on their size. However if the size of the solid becomes very small, its properties do in fact depend on the size.[46] This quantum size effect will be important if the size of the nanocrystal becomes of the same order as the exciton Bohr radius. The electron energy levels can no longer be treated as continuous, as in bulk semiconductors, but must be treated as discrete electronic states (the quantum confinement effect). Therefore by controlling the size of a nanocrystal on the nanometre scale, its properties can be tailored.

Essential for the optical properties of a nanocrystal are its energy levels, which can be derived from the free-particle Schrödinger equation [8]

$$-\frac{\hbar^2}{2\,m}\,\nabla^2\mathbf{r}\;\Psi_{\mathbf{k}}(\mathbf{r}) = E_{\mathbf{k}}\;\Psi_{\mathbf{k}}(\mathbf{r})\,. \tag{9}$$

Wavefunctions that satisfy the Schrödinger equation and the imposed periodic boundary conditions are of the form of a travelling plane wave

$$\Psi_{\mathbf{k}}(\mathbf{r}) = e^{(i\,\mathbf{k}\bullet\mathbf{r})} \tag{10}$$

provided that the components of the wavevector **k** satisfy

$$k_{x,y,z} = \pm\frac{2\,n\,\pi}{L}\,, \tag{11}$$

with n is any integer and L the length over which the electrons are confined, i.e. the size of the nanocrystal. Substituting the wavefunction in the Schrödinger equation gives the energy as

$$E_{\mathbf{k}} = \frac{\hbar^2\,k^2}{2\,m} = \frac{\hbar^2\left(k_x^2 + k_y^2 + k_z^2\right)}{2\,m}\,. \tag{12}$$

Combining equation 11 and equation 12 shows that the energy levels depend on the size of the nanocrystal as $E_{\mathbf{k}} \sim L^{-2}$. Both the electron energy levels in the conduction band and the hole energy levels in the valence band are quantized in this manner. Therefore the electron energy levels increase with decreasing size of the nanocrystal. On the other hand the hole energy levels decrease with decreasing size of the nanocrystal. In this way the band gap energy can be increased by decreasing the size of the nanocrystal.[8] So by changing the size of the nanocrystal it is possible to tune the band gap energy and the corresponding optical properties.

5.2 Synthesizing nanocrystal structures

Nanocrystal structures can be made by physical methods like molecular beam techniques or complicated lithographic techniques. For the purpose of sensitizing polymers these methods are however not very suitable. Fortunately some nanocrystals can also be made by methods of colloidal chemistry, in which materials spontaneously form nanocrystals. These methods allow for production of stable colloids of nanocrystalline particles that can be processed and handled easily like normal chemical substances.

Many synthetic routes are described in literature. Various II-VI nanocrystals (CdS, CdSe, CdTe,

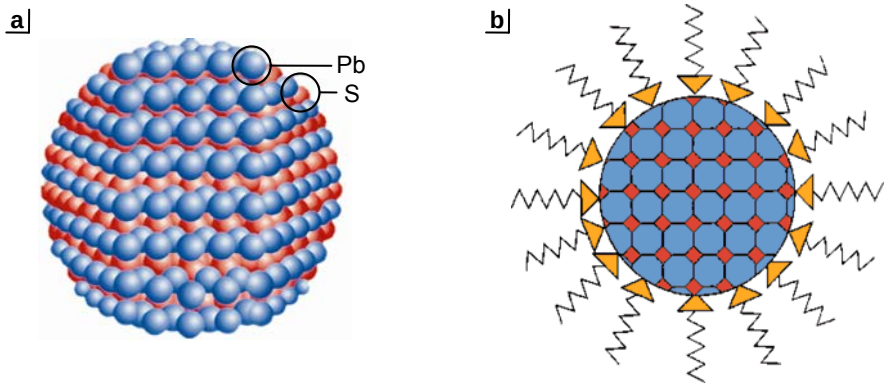

Figure 9 – Nanocrystals. a) Artistic impression of a PbS nanocrystal. (adapted from http://www.evidenttech.com) b) A PbS nanocrystal capped by organic ligands consisting of a hydrocarbon chain and an end functional group. (adapted from [53])

$Cd_xHg_{1-x}Te$, HgTe) can be synthesized in aqueous solutions by the metathesis reaction in the presence of different thiols.[47, and references therein] The thiols function as stabilizing agents and allow control over the nanocrystal size during synthesis. Better crystallinity and narrower size distributions of the nanocrystals can be obtained by high-temperature thermolysis of organometallic precursors in mixtures of high-temperature-boiling coordinating solvents to prepare CdSe and CdTe.[47, and references therein] Nanocrystals of III-V compounds (InP, InAs) can be prepared by a dehalosylilation reaction, again in high-temperature-boiling coordinating solvents.[47, and references therein] In this reaction the nanocrystal size is controlled by the reaction temperature. Several metal sulphide nanocrystals (PbS, ZnS, CdS, MnS) have been synthesized from a thermal reaction of metal chlorides and elemental sulphur in oleylamine.[48] This synthetic method is a general process and can be applied to synthesize different kinds of sulphide nanocrystals. It results in uniform-sized nanocrystals without the need for a further size-selection process.
Another synthetic route for the production of narrowly dispersed colloidal lead sulphide nanocrystals is commonly employed.[49] This solution phase organometallic method uses cost-effective and non-pyrophoric precursors and gives stable and processible nanocrystals. Nanocrystal size can be tuned

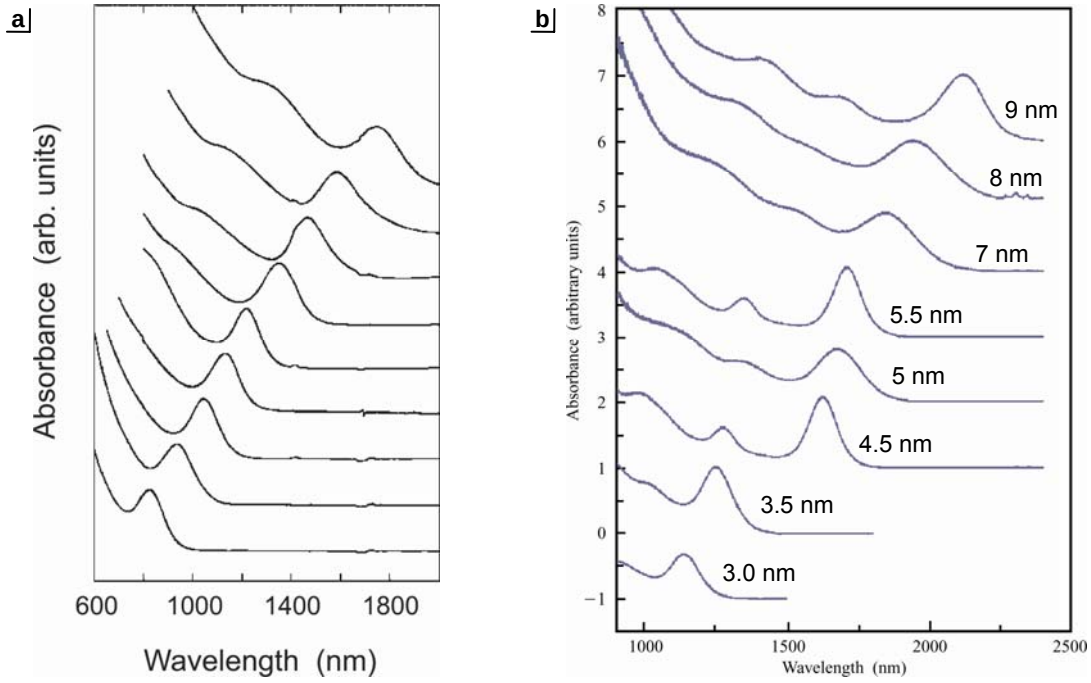

Figure 10 – Tunability of nanocrystal absorption spectra. a) Room-temperature optical absorption spectra of toluene solutions of PbS nanocrystals spanning the range of tunable sizes. Corresponding sizes not reported. (after [49]) b) Room-temperature optical absorption spectra for a series of PbSe nanocrystals. (after [50])

by variations in reaction parameters with narrow size dispersions without the need for any post-synthesis size selection. This results in absorption spectra being tuned accordingly (Fig 10a). Another often used nanocrystal, lead selenium, is generally produced via a high-temperature solution phase synthesis.[50, and references therein] Solution temperature is used to tune the size of the PbSe nanocrystals. A size-selective precipitation is performed to further narrow the size distribution. Again by tuning the size of the nanocrystals the absorption spectra are tuned accordingly (Fig 10b). The same narrow size distribution of PbSe nanocrystals can be obtained without size-selective precipitation by using a non-coordinating solvent.[51] This method eliminates the use of toxic organometallic precursors and phosphine containing solvents.
The synthesized nanocrystals have to be dispersed in a polymer to sensitize it. To get a good dispersion and to prevent aggregation the nanocrystals have to be capped with an organic ligand (Fig 9b).[52] Some synthetic procedures gives ligand capped nanocrystals by itself; [47, 49, 50] other procedures do not [48, 51]. To observe the photoconductive effect charge transfer must be possible between nanocrystals and polymer, so intimate electronic contact of the nanocrystals with the polymer is essential. Using an oleic acid ligand such electronic contact is still possible. The conformation of single chain ligands on the high curvature nanocrystal surfaces still leaves spaces making the surface accessible for electronic contact by the polymer.[54] Some ligands introduced by the nanocrystal synthesis itself however do not facilitate good electrical contact. In these cases it is possible to replace the ligands with a shorter alkyl amine chain, thereby also reducing the thickness of the insulating capping layer.[47, 55]
With the aforementioned methods nanocrystals are synthesized first and then blended with a polymer. For lead sulphide it is however also possible to synthesize the nanocrystals directly in the polymer by a one pot process.[56, 57, 58] This eliminates the necessity of a capping layer for mixing and blending and is therefore a simple but suitable technique for photoconductive nanocrystal–polymer composites. With a recent novel method [59] it is even possible to obtain monodisperse nanocrystals just as with the older two-step methods.

6 – Infrared photoconductivity of nanocrystal-sensitized polymers

The first results about infrared photoconductivity of nanocrystal-sensitized polymers were published by Steven McDonald and co-workers from the group of Edward Sargent at the University of Toronto.[24, 60] Shortly after also Kaushik Roy Choudhury and co-workers, from the group of Paras Prasad at the State University of New York at Buffalo, published their contributions to this field of research.[54, 61, 62] Until today these two groups are the only players in the field of infrared photoconductivity of nanocrystal-sensitized polymers that published any data.

6.1 PbS nanocrystal–MEH-PPV composites

McDonald *et al*. demonstrated photoconductivity in the infrared region of the electromagnetic spectrum using a composite of lead sulphide (PbS) nanocrystals in MEH-PPV (Fig 11a).[24, 60] PbS as the nanocrystal material in a nanocrystal–polymer composite is however not an easy choice. To observe the photoconductive effect it is important that exciton dissociation occurs as explained before. Organic conjugated polymers typically have better hole conduction than electron conduction. To obtain the photoconductive effect it is therefore important that the energy alignment of the nanocrystal with respect to the polymer is such that it favours transfer of the photogenerated hole to the polymer. This requires that the top of the valence band of the polymer lies closer to vacuum than the valence band of the PbS nanocrystal. The bulk ionization potential of PbS is ~4.95 eV. Most polymers however have ionization potentials larger than ~5.3 eV,[24, and reference therein] so this limits the number of readily available conjugated polymers. Therefore McDonald *et al*. used the polymer MEH-PPV which has the top of its valence band between ~4.9 and ~5.1 eV [24, 60, and references therein] providing a favourable energy alignment (Fig 12).
McDonald *et al*. synthesized their PbS nanocrystals via the solution phase organometallic approach [49] and performed a post synthetic ligand exchange to obtain shorter octylamine ligands [55]. The PbS

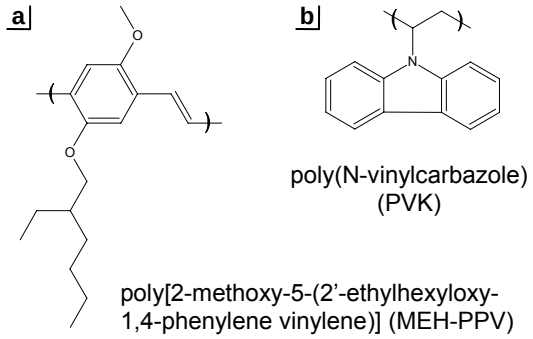

Figure 11 – Structures of the two polymers used for infrared photoconduction. a) MEH-PPV b) PVK

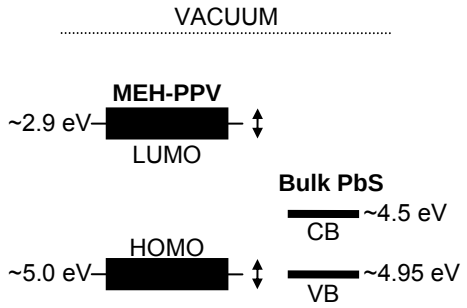

Figure 12 – Energy levels alignment of PbS and MEH-PPV. The top of the valence band of MEH-PPV (HOMO: highest occupied molecular orbital) is reported around 5.0 eV and the ionization potential of bulk PbS around 4.95 eV. The arrows represent the uncertainty in the energy levels of MEH-PPV. As long as the top of the valence band of MEH-PPV lies above the valence band of PbS transfer of the photogenerated holes is favourable. (reproduced after [60])

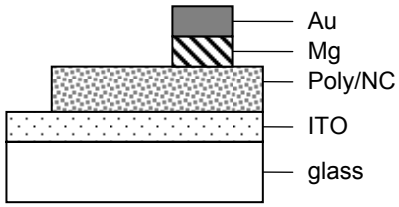

Figure 13 – Device structure used by McDonald *et al*. A layer of indium tin oxide (ITO) on a glass substrate covered with a spin-coated film of the PbS nanocrystal–MEH-PPV (Poly/NC) composite. Magnesium (Mg) electrodes covered with a gold (Au) capping layer were deposited on top. (reproduced after [60])

nanocrystals were dispersed in toluene or chloroform and combined with a solution of MEH-PPV. The composite solution was spin-coated onto a layer of indium tin oxide (ITO) after which magnesium contacts and a gold capping layer were deposited on top of the device (Fig 13).[60]
From absorption spectra (Fig 14) of the PbS nanocrystal solution, pure MEH-PPV films and PbS nanocrystal–MEH-PPV composite it can be seen that the nanocrystals sensitize the polymer into the infrared region of the electromagnetic spectrum. They both increase the sensitivity in the visible region (chemical sensitization) and extend the sensitivity into the infrared region (spectral sensitization). Application of a voltage across the device upon illumination with a 975 nm pump laser at ~90 mW pump power showed a photocurrent, indicative for the photoconductive effect taking place. The photocurrent increased up to ~5.3 nA with applied bias reaching 6 V with a photocurrent to dark current ratio of ~10^{-4}.[60] Measurements of this photocurrent versus pump intensity at 5 V bias showed a nearly linear behaviour, resulting in a internal quantum efficiency of photogeneration of 10^{-6} to 10^{-5} charges/photon (~0.005 %).[60] This low internal quantum efficiency and the low photocurrent to dark current ratio necessitated the use of modulated illumination (50 kHz) and a lock-in amplifier to observe the photocurrent signal.

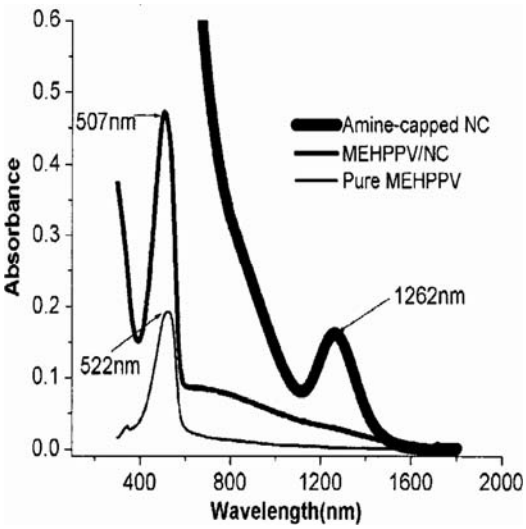

Figure 14 – Absorption spectra of PbS and MEH-PPV. Absorption spectra for octylamine-capped PbS nanocrystals in solution (thick weight), PbS nanocrystal–MEH-PPV composite on ITO (medium weight) and pure MEH-PPV on ITO (thin weight). The PbS nanocrystals provide both chemical sensitization and spectral sensitization of MEH-PPV. (after [60])

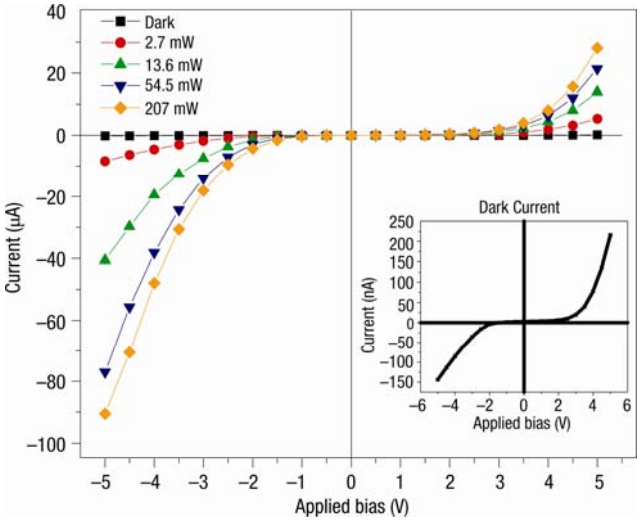

Figure 15 – Photocurrent of PbS nanocrystal–MEH-PPV composite. Dark current and photocurrent versus applied bias voltage under illumination of a 975 nm continuous-wave laser for different incident powers. The inset shows an enlargement of the dark current versus applied bias voltage. At a bias of -5 V the photocurrent to dark current ratio was determined at 59 and 630 for 2.7 mW and 207 mW incident power respectively. [24]

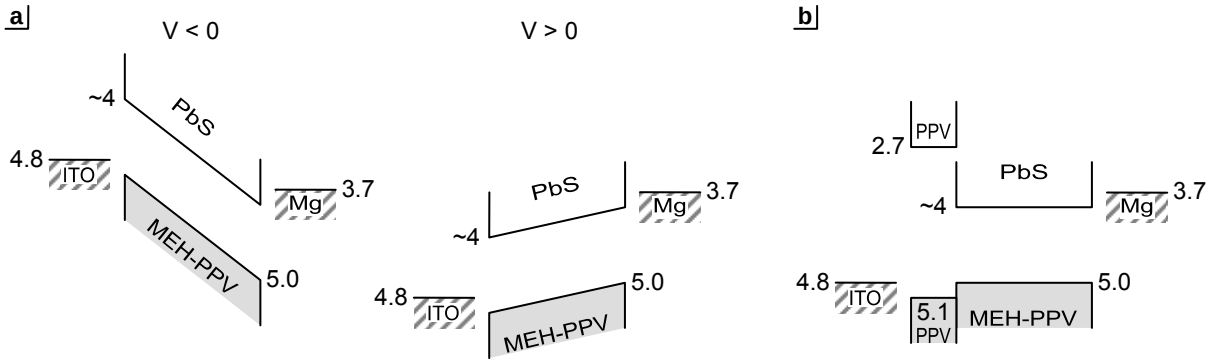

Figure 16 – Origin of asymmetric photocurrent curve. a) Generally asymmetry is due to a work function difference between the electrodes (ITO: ~4.8 eV, magnesium: 3.7 eV). When a negative voltage is applied to the ITO electrode (left), photogenerated electrons are extracted from the magnesium electrode. Before they can be extracted they have to overcome however an electron barrier of ~0.3 eV. Electrons injected from the ITO electrode need to overcome an energy barrier of 0.8 eV. When a positive voltage is applied (right), the photogenerated electrons are extracted from the ITO electrode. There is neither an energy barrier present for extraction nor for electron injection at the magnesium electrode. The photocurrent under positive applied bias voltage would therefore be larger than the photocurrent under negative applied bias voltage. This results in an asymmetric photocurrent curve opposite to the measurements of McDonald *et al*. b) Energy levels of the device including the PPV layer. The electron barrier posed by the PPV layer (~1.3 eV) is higher than the hole barrier (0.1 eV) resulting in an asymmetric photocurrent as measured by McDonald *et al*. The conduction band of MEH-PPV and the valence band of PbS have been omitted for convenience, since these levels do not contribute directly to free charge carrier transport. (data taken from [24])

In search for better performances McDonald *et al*. developed an improved device obtaining a higher quantum efficiency of photogeneration and larger photocurrent to dark current ratios.[24] This allowed for observation of the photocurrent under continuous-wave illumination without the need for lock-in techniques. The higher quantum efficiency of photogeneration was attributed principally to an improvement in film quality.[24] First of all the device consisted of an extra layer of poly(*p*-phenylenevinylene) (PPV) between the ITO layer and the PbS nanocrystal–MEH-PPV composite. This PPV layer acted as a hole transport layer and provided better electrical stability eliminating shorts directly from the ITO to the magnesium contact. Second, the MEH-PPV was ultrasonificated before spin-coating the film and both MEH-PPV and PbS nanocrystal solutions were filtered independently. These treatments resulted in smoother films: smaller regions of aggregated, transport hindering material and free of pinholes. These improved films allowed better interfacial contact with the magnesium electrode, resulting in better carrier extraction.[24, and reference therein] PPV also introduced an injection barrier for electrons at the ITO electrode. This reduced the dark current and therefore increased the photocurrent to dark current ratio.

The photocurrent as a function of applied bias voltage had been measured under illumination of a 975 nm continuous-wave laser for different incident powers (Fig 15).[24] At a bias of -5 V the photocurrent to dark current ratio was determined at 59 and 630 for 2.7 mW and 207 mW incident power respectively. These larger on/off ratios compared to the first work of McDonald *et al*. are of critical importance for detection and imaging applications.

The photocurrent curves show a clear asymmetry with higher photocurrents at negative voltages than at positive voltages. McDonald *et al*. ascribe this asymmetry partially to the work function difference between the electrodes, as is generally the case (Fig 16a). In the case of ITO and magnesium, with a work function of ~4.8 eV and 3.7 eV respectively, this would however give an opposite asymmetry (higher photocurrents at positive voltages than at negative voltages). In reality the asymmetry is due to the energy levels of the PPV layer. PPV has an ionization energy of ~5.1 eV and an electron affinity of ~2.7 eV [24, and reference therein]. When a negative bias voltage is applied, holes travel to the ITO electrode and have to overcome an energy barrier of 0.1 eV to enter the PPV layer. When a positive bias voltage is applied, electrons travel to the ITO and they have to overcome an energy barrier of ~1.3 eV to enter the PPV layer (Fig 16b). The electron barrier posed by the PPV layer is higher than the hole barrier in free charge carrier extraction, so application of a negative voltage gives a higher photocurrent. The asymmetric photocurrent curve as measured by McDonald *et al*. therefore must be strictly due to the PPV layer.

The reported photocurrent versus incident power at a fixed applied bias voltage does not increase linearly. At higher incident power the photocurrent increases more slowly with increased power. In the low power region, the recombination of trapped electrons in the PbS nanocrystal with holes in the

neighbouring MEH-PPV dominates. At high power, more photons are absorbed and bimolecular recombination between free holes and free electrons starts to occur. This additional bimolecular recombination reduces the number of free charge carriers and the photocurrent starts to saturate. A constant photocurrent with increasing incident power therefore results in a lowering of internal quantum efficiency. Whereas the average internal quantum efficiency is 3 % in the low-power region, it is reduced to 0.4 % at 207 mW.[24] Nevertheless, these internal quantum efficiencies are still much larger than the first reported value.

To prove the tunability of the photoconductive effect by changing the sizes of the nanocrystals, McDonald *et al*. measured the photocurrent for three samples with different PbS nanocrystal size.[24] The photocurrents were measured for all wavelengths between 700 nm and 1800 nm obtaining photocurrent spectral responses (Fig 17). The sizes of the PbS nanocrystals were chosen such that the absorption peaks were tuned to 955 nm, 1200 nm and 1355 nm respectively. It is clear that the photocurrent spectral responses correspond with the absorption peaks of the PbS nanocrystal–MEH-PPV composites. At wavelengths longer than 600 nm the absorption of MEH-PPV is negligible (see also Fig 14), so all absorption can be assigned to the PbS nanocrystals. It therefore demonstrates not only tunability of the photocurrent spectral response, but also that the photocurrent is due to exciton formation in the PbS nanocrystals followed by charge separation.

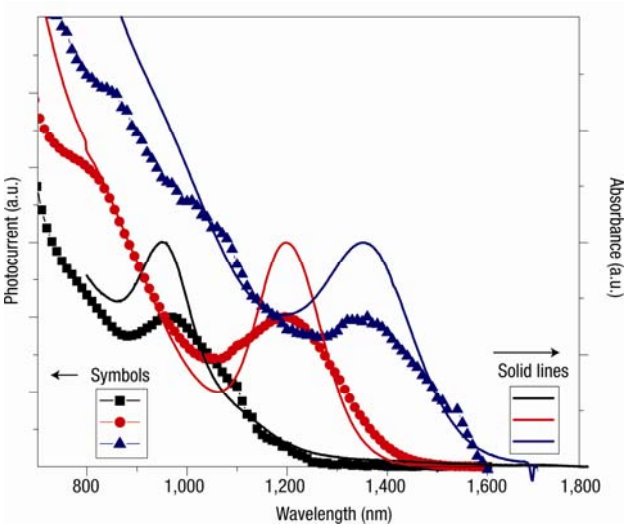

Figure 17 – Photocurrent spectral responses. Photocurrent spectral responses (symbols) and the corresponding absorption spectra (solid lines) for three samples with different PbS nanocrystal size. The sizes of the PbS nanocrystals were chosen such that the absorption peaks were tuned to 955 nm (black), 1200 nm (red) and 1355 nm (blue). (after [24])

6.2 PbS nanocrystal–PVK composites

Roy Choudhury *et al*. fabricated a similar device with PbS nanocrystals in PVK (Fig 11b).[61] The PbS nanocrystals were synthesized however using a different procedure [48, 61] and aluminium contacts were used instead of magnesium contacts. The ionization potential of PVK is ~5.4 eV [54, and reference therein]. According to the energy level alignments a small energy barrier has to be overcome for hole transfer from PbS nanocrystals to PVK to occur (compare Fig 12). Nevertheless, Roy Choudhury *et al*. were able to measure a photoconductive effect. Apparently it is not a problem to overcome the energy barrier for hole transfer to PVK. It might also be that PbS nanocrystals have different energy levels than bulk PbS in such a way that there is no energy barrier at all.

Roy Choudhury *et al*. reported their results like photosensitivity as a function of applied field. The photosensitivity S_{ph} was calculated from the photocurrent density J_{ph} using the illumination intensity of the incident laser beam I by [61]

$$S_{ph}\left[\frac{\mathrm{M}}{\Omega\,\mathrm{W}}\right] = \frac{J_{ph}[\mathrm{A}]}{E\left[\frac{\mathrm{V}}{\mathrm{m}}\right] I[\mathrm{W}]}\,. \qquad (13)$$

Values reported ranged from ~1x10^{-13} to ~1.6x10^{-12} cm/ΩW for applied electric fields of ~30 V/μm up to ~115 V/μm. Unfortunately, Roy Choudhury *et al*. do not mention which illumination intensity has been used. To compare with the work of McDonald *et al*. the photocurrents of the latter have to be converted to photosensitivity. Using a typical value of 90.61 μA at -5 V at an incident power of 207 mW on a 100 nm thick sample (data from [24]) the photosensitivity is in the order of 10^{-10} cm/ΩW. At this applied electric field (50 V/μm) the values of McDonald *et al*. are already two orders of magnitude higher than any of the values reported by Roy Choudhury *et al*. So it might be concluded that PbS nanocrystals are better in sensitizing MEH-PPV than PVK with respect to the photoconductive effect.

It has to be mentioned however that Roy Choudhury *et al*. also used a plasticizer and a chromophore in their PbS nanocrystal–PVK composite, because their work focused on photorefractive composites. It may therefore be expected that these compounds influenced the photoconductivity and that Roy Choudhury *et al*. did not optimize their devices with respect to the photoconductive effect.

6.3 PbSe nanocrystal–PVK composites

Another approach to infrared sensitization of PVK is the use of lead selenium (PbSe) nanocrystals instead of lead sulphide. Roy Choudhury *et al*. explored this option and published two articles about such a composite.[54, 62] The PbSe nanocrystals were synthesized by making some variations to existing literature methods [51, 54, 62] and similar devices as before with aluminium electrodes were fabricated. The ionization potential reported for bulk PbSe ranges between ~8.4 eV and ~8.8 eV [54, and reference therein]. This makes the hole transfer possible again without any energy barrier to overcome.

The first report of Roy Choudhury *et al*. was again as part of the search for photorefractive composites. The photocurrent as a function of applied bias voltage had been measured under illumination of a 1550 nm continuous-wave laser at 50 mW incident power (Fig 18a).[62] The photocurrent at an applied bias voltage of -25 V was 71.96 nA, while the dark current was 0.1 nA. This results in a photocurrent to dark current ratio of 720. At first glance this looks better than the reported 630 of McDonald *et al*. It has to be taken in mind however that this latter value had been determined at -5 V applied bias voltage. It is very hard to determine the photocurrent at -5 V from the curve of Roy Choudhury *et al*., but a very positive guess is 5 nA. This would result in a photocurrent to dark current ratio of only 50; much lower than the result reported by McDonald *et al*.

Again an asymmetric photocurrent curve can be observed. Roy Choudhury *et al*. also used electrodes with different work functions (ITO: ~4.8 eV, aluminium: ~4 eV). From these values it would be expected to observe the asymmetry in the opposite way. Possibly Roy Choudhury *et al*. applied the bias voltage to the aluminium electrode instead of the ITO electrode, but this is not clear from their report. Nevertheless a quantum efficiency of photogeneration up to ~0.65 % at the highest operational bias was possible to reach.

Roy Choudhury *et al*. published a second report focussing on the photoconductive effect. The devices described in this report did not contain the plasticizer and chromophore anymore and the concentration of PbSe nanocrystals in the composite had been increased from ~10 weight percent to ~40-50 weight percent. Thanks to these changes Roy Choudhury *et al*. were able to increase the quantum efficiency of photogeneration to ~3 % at the maximum applied bias voltage of 34 V.[54] The photocurrent as a function of applied bias voltage had been measured under illumination of a 1340 nm and 1550 nm continuous-wave laser respectively at two sample with different PbSe nanocrystal size (Fig 18b).[54] The photocurrents at the maximum applied bias voltage of 34 V were 144 nA and 164 nA for the samples sensitized at 1340 nm and 1550 nm respectively, while the corresponding dark currents were 19 nA and 34 nA. This results in a photocurrent to dark current ratio of 8 and 5 respectively. Compared to the first report of Roy Choudhury *et al*. on PbSe nanocrystal– PVK composites these values are extremely low. The photocurrents are larger than before, but also the dark currents are much larger. Apparently increasing the PbSe nanocrystal concentration in the composite influences the dark current more than the photocurrent, although this is not easily rationalized. It seems like the dark current is magnified again as in the first publication on PbSe, which would explain the higher dark current. This is however not reported anywhere in the article.

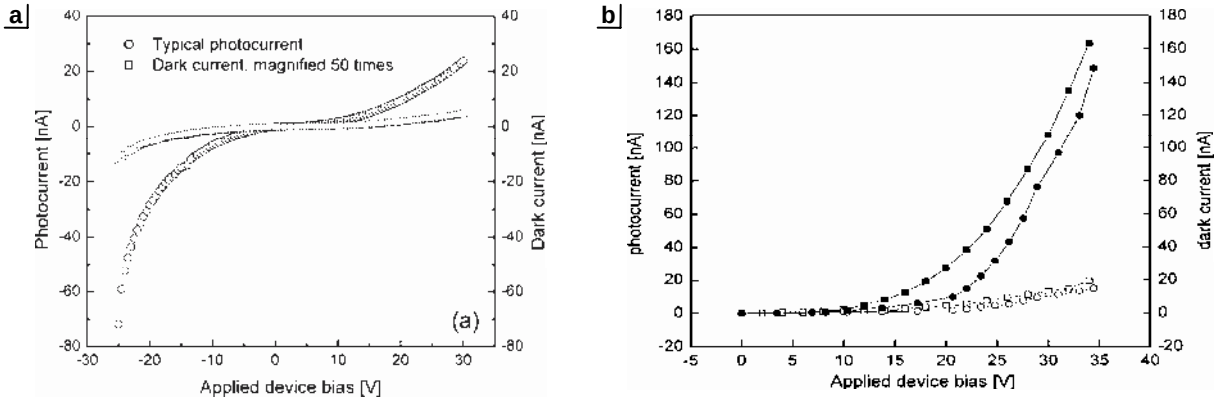

Figure 18 – Photocurrents of PbSe nanocrystal–PVK composites. a) Dark current (squares) and typical photocurrent (circles) as a function of applied bias voltage under illumination of a 1550 nm continuous-wave laser at 50 mW incident power. [62] b) Dark currents (open symbols) and photocurrents (filled symbols) as a function of applied bias voltage under illumination of a 1340 nm (circles) and 1550 nm (squares) continuous-wave laser of two sample with different PbSe nanocrystal size. [54]

6.4 Comparing the different composites

Compared to each other McDonald *et al*. reports the best results so far. Roy Choudhury *et al*. claim equal performance especially of quantum efficiency of photogeneration. They forget however that the ~3 % quantum efficiency of McDonald *et al*. had been obtained at -5 V applied bias voltage, whereas their own result had been obtained at 34 V. At 5 V applied bias voltage Roy Choudhury *et al*. obtained a quantum efficiency of photogeneration of less than 0.1 %.[54] Apart from this the composites of Roy Choudhury *et al*. also show much lower photocurrent to dark current ratios. These on/off ratios are however of critical importance for detection and imaging applications. In addition the reports of Roy Choudhury *et al*. show some indistinctness and inconsistencies, e.g. some aspects of the photosensitivity, the high dark current and the opposite asymmetry in the photocurrents.

It may be possible to increase the photocurrents and quantum efficiencies of photogeneration of the composites of Roy Choudhury *et al*. by further increasing the nanocrystal concentrations. This might increase the efficiency of charge transport without recombination by formation of a percolating network giving an appropriate pathway for electron conduction.[45, 54]

Regardless of the lower performances of their devices, Roy Choudhury *et al*. were able to sensitize a polymer further into the infrared region than McDonald *et al*. (1550 nm compared to 975 nm). McDonald *et al*. showed however that they were able to tune the photocurrent spectral response of their devices by using PbS nanocrystals of different sizes.[24] As have been reported, PbS nanocrystals have absorption peaks that can be tuned from ~800 nm to ~2000 nm.[49] It is therefore expected that McDonald *et al*. will also be able the extend the sensitization of their devices further into the infrared region. The same however counts for the PbSe nanocrystals that can be tuned from ~1100 nm to ~2200 nm [63].

The nanocrystals used have potential tunability up to ~3600 nm (PbS) and ~4500 nm (PbSe) as can be inferred from the bulk band gap energies (see Table 1). For most applications however sensitization up to 4500 nm is not necessary. A high photocurrent to dark current is of much more importance for most applications. From the current state it can therefore be concluded that PbS nanocrystal–MEH-PPV composites are a better choice than PbSe nanocrystal–PVK composites.

7 – Infrared photoconductivity of solution-processed nanocrystals

A few groups published about infrared photoconductivity from nanocrystal films processed from solution.[64-67] In these experiments nanocrystals are processed from solution like polymers, allowing convenient integration with any substrate, without the need for a polymer. Moreover, in contrast to bulk material, their sizes can still be tuned, keeping the possibility of tuning the spectral responses by means of the quantum size effect.

One publication reports about PbS nanocrystals spin-coated from solution onto a glass substrate coated with gold electrodes.[64] PbS nanocrystals were prepared by the commonly used synthesis [49], but the resulting oleic acid capped PbS nanocrystals were found to be insulating. Therefore a ligand exchange was performed [64], resulting in a photoconductive effect. The response depended on an oxidation step during fabrication, as a result of trap-state-forming oxides, and on the interparticle separation, as a result of crosslinking between adjacent nanocrystals.

Two other publications described mercury tellurium (HgTe) nanocrystals, either bare or capped with thioglycerol, dropped from an aqueous solution.[65, 66] The thioglycerol capped nanocrystals were synthesized by a colloidal method and either directly dropped onto silicon substrates [65] or first treated to remove the organic capping ligands, re-dispersed in water and then dropped on substrates [66]. A photocurrent was observed under illumination of light with wavelengths up to 1050 nm. The thioglycerol ligands were thought to act as a hole transport medium, whereas the electrons were trapped at the HgTe nanocrystal

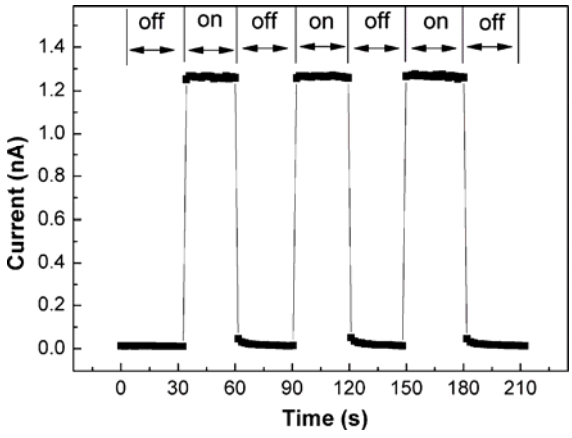

Figure 19 – On-off behaviour of HgTe nanocrystals. Very clear on-off behaviour of a film of uncapped HgTe nanocrystals, dropped from an aqueous solution between gold electrodes on a silicon substrate, due to light of 1100 nm at an applied bias voltage of 3 V. [66]

centres.[65] To reduce dark currents the thioglycerol ligands were removed. The dark current became negligible indeed, but also the photocurrent decreased dramatically, yet it was still three orders of magnitude higher than the dark current.[66] The photocurrent spectral response extended up to 1800 nm and a very clear on-off behaviour could be observed (Fig 19).
Finally a not yet published article reports about an infrared photoconductor of inkjet-printed nanocrystals.[67] Inkjet-printing is a powerful tool for very accurate deposition of liquids containing suspended nanocrystals. By using HgTe sensitivity up to a wavelength of 3 μm could be achieved. Nanocrystals were synthesized in aqueous solution and afterwards a ligand exchange was performed.[67] For inkjet-printing the viscosity and surface tension of the liquid are very important. Therefore HgTe nanocrystals were suspended in chlorobenzene to obtain optimal droplet ejection. Large photocurrents compared to dark current could already be observed under illumination with a power of 42 μW. Also PbSe nanocrystals were studied for their sensitivity up to μm wavelengths. PbSe nanocrystals however showed a significantly faster degradation with time.[67] Therefore HgTe nanocrystals were used to obtain photoconduction at even larger wavelengths by varying the size of the nanocrystals.

8 – Conclusion and further prospects

Infrared photoconductivity of nanocrystal-sensitized polymers is still in its infancy. Only a few results have been published so far with photoconductivity really extending into the infrared region of the electromagnetic spectrum. The use of nanocrystals however offers a large freedom in tunability of the absorption peak of nanocrystal–polymer composites, only limited by the bulk value of the band gap energy. One problem that might arise however is the optical quality of the nanocrystals that significantly decreases with increasing nanocrystal size [67]. Some promising materials like PbS and PbSe, but also HgTe, have been studied; others are theoretically still an interesting option.
MEH-PPV and PVK are used at the moment as hole transporting medium in the composite. The energy levels of these polymers have the best alignment to the nanocrystals used so far. Using other nanocrystals, more readily available polymers might be suitable for composite formation. Incorporation of charge transport layers or changing and removing the capping ligand around the nanocrystal also might improve charge transfer, although processability may be reduced. Other approaches relying on nanocrystals spin-coated, dropped or inkjet-printed directly from solution are interesting ways of improvement of photoconductivity and processability. The use of polymers may nevertheless be preferred due to the flexibility of the final material.
As long as a high photocurrent to dark current ratio can be obtained with low incident power, low applied bias voltage and a consequently high quantum efficiency of photogeneration any of the approaches described could become the best option. Nevertheless, still a lot of work has to be done to reach the level of cost-efficient, easy to process and high-performance infrared photoconductive materials ready to use for relevant applications.

Acknowledgement

I would like to thank my supervisor Dr. Maria Antonietta Loi for giving me an interesting set of publications as a starting point for this paper project.

References

[1] J.N. Mait, *A history of imaging: Revisiting the past to chart the future*, Optics and Photonics News **17**, 22–27 (2006)
[2] A.E. Becquerel, Compt. Rend. Acad. Sci. **9**, 145 (1839)
[3] A.E. Becquerel, Compt. Rend. Acad. Sci. **9**, 561 (1839)
[4] H. Spanggaard and F.C. Krebs, *A brief history of the development of organic and polymeric photovoltaics*, Sol. Energy Mater. Sol. Cells **83**, 125–146 (2004)
[5] W. Smith, *Effect of light on selenium during the passage of an electric current*, Nature **7**, 303 (1873)
[6] W.G. Adams and R.E. Day, *The action of light on selenium*, Proc. R. Soc. London **25**, 113–117 (1876)
[7] A. Rogalski, *Infrared photon detectors*, SPIE Optical engineering press, 644 pp. (1995)
[8] C. Kittel, *Introduction to solid state physics, eight edition*, John Wiley & Sons, 680 pp. (2005)
[9] S.M. Sze, *Physics of semiconductor devices, second edition*, John Wiley & Sons, 868 pp. (1981)
[10] A.H.W. Beck and H. Ahmed, *An introduction to physical electronics*, Edward Arnold Publishers, 360 pp. (1968)

[11] A. van der Ziel, *Solid state physical electronics*, Englewood Cliffs, 604 pp. (1957)
[12] J.A. Chilton and M.T. Goosey (ed.), *Special polymers for electronics and optoelectronics*, Chapman & Hall, 351 pp. (1995)
[13] B. de Boer, Lectures and lecture notes *Opto-electronic properties of polymers*, Zernike institute for advanced materials, University of Groningen, (2007)
[14] P.W.M. Blom, Lectures and lecture notes *Physics of organic semiconducting devices*, Zernike institute for advanced materials, University of Groningen (2007)
[15] S. Rawlings, M. Lacy, K.M. Blundell, S. A. Eales, A.J. Bunker, S.T. Garrington, *A radio galaxy at redshift 4.41*, Nature **383**, 502–505 (1996)
[16] R. Schödel, T. Ott, R. Genzel, R. Hofmann, M. Lehnert, A. Eckart, N. Mouawad, T. Alexander, M.J. Reidk, R. Lenzen, M. Hartung, F. Lacombe, D. Rouan, E. Gendron, G. Roussetq, A.-M. Lagrange, W. Brandner, N. Ageorges, C. Lidman, A.F.M. Moorwood, J. Spyromilio, N. Hubin, K. M. Menten, *A star in a 15.2-year orbit around the supermassive black hole at the centre of the Milky Way*, Nature **419**, 694–696 (2002)
[17] M. Strojnik, G. Paez, *Infrared detection of a planet next to a bright star*, Infrared Phys. Technol. **49**, 312–316 (2007)
[18] N. Cohen, A. Zussman, G. Sarusi, *A monolithic LWIR/NIR multispectral QWIP for night vision and see spot*, Infrared Phys. Technol. **42**, 391–396 (2001)
[19] A. Goldberg, P.N. Uppal, M. Winn, *Detection of buried land mines using a dual-band LWIR/LWIR QWIP focal plane array*, Infrared Phys. Technol. **44**, 427–437 (2003)
[20] M. Ettenberg, *A little night vision: InGaAs shortwave infrared emerges as key complement to IR for military imaging*, Adv. Imaging **20**, 29–32 (2005)
[21] E.H. Sargent, *Infrared quantum dots*, Adv. Mater. **17**, 515–522 (2005)
[22] Y.T. Lim, S. Kim, A. Nakayama, N.E. Stott, M.G. Bawendi, J.V. Frangioni, *Selection of quantum dot wavelenghts for biomedical assays and imaging*, Molecular Imaging **2**, 50–64 (2003)
[23] S. Kim, Y.T. Lim, E.G. Soltesz, A.M. De Grand, J. Lee, A. Nakayama, J.A. Parker, T. Mihaljevic, R.G. Laurence, D.M. Dor, L.H. Cohn, M.G. Bawendi, J.V. Frangioni, *Near-infrared fluorescent type II quantum dots for sentinel lymph node mapping*, Nat. Biotechnol. **22**, 93–97 (2004)
[24] S.A. McDonald, G. Konstantatos, S. Zhang, P.W. Cyr, E.J.D. Klem, L. Levina, E.H. Sargent, *Solution-processed PbS quantum dot infrared photodetectors and photovoltaics*, Nat. Mater. **4**, 138–142 (2005)
[25] D. Han and L. Wu, *Infrared stimulated photoconductivity overshoot in a-Si:H*, J. Appl. Phys. **67**, 3717–3723 (1990)
[26] A.I. Yakimov, A.V. Dvurechenskii, Y.Y. Proskuryakov, A.I. Nikiforov, O.P. Pchelyakov, S.A. Teys, A.K. Gutakovskii, *Normal-incidence infrared photoconductivity in Si p-i-n diode with embedded Ge self-assembled quantum dots*, Appl. Phys. Lett. **75**, 1413–1415 (1999)
[27] J. Bandaru, J.W. Beeman, E.E. Haller, S. Samperi, N.M. Haegel, *Influence of the Sb dopant distribution on far infrared photoconductivity in Ge:Sb blocked impurity band detectors*, Infrared Phys. Technol. **43**, 353–360 (2002)
[28] H. Nakataa, A. Yokoyamaa, N. Tsubouchib, K. Fujii, *Nonlinear infrared photoconductivity in Ge doped with As or Zn*, Physica B **376–377**, 220–223 (2006)
[29] R.E.M. de Bekker, J.M. Chamberlain, L.M. Claessen, P. Wyder, M.B. Stanaway, R.T. Grimes, M. Henini, O.H. Hughes, G. Hill, *Subnanosecond far infrared photoconductivity from a GaAs/AlGaAs multiquantum well*, J. Appl. Phys. **68**, 1913–1915 (1990)
[30] S.H. Hwanga, J.C. Shina, J.D. Songa, W.J. Choia, J.I. Leea, H. Han, *Detection wavelength tuning of InGaAs/GaAs quantum dot infrared photodetector with thermal treatment*, Microelectron. J. **36**, 203–206 (2005)
[31] S.R. Forrest, *The path to ubiquitous and low-cost organic electronic appliances on plastic*, Nature **428**, 911–918 (2004)
[32] Y. Lee, S. Sadki, B. Tsuie, P. Schottland, J.R. Reynolds, *A new silole containing low band gap electroactive polymer*, Synth. Met. **119**, 77–78 (2001)
[33] Q. Zhang, M. Yang, P. Wu, H. Ye, X. Liu, *Synthesis and characterization of a low band gap polymer with an aromatic oxadiazole moiety as the side chain*, Synth. Met. **156**, 135–140 (2006)
[34] H. Meng, Y. Chen, F. Wudl, *A robust low band gap processable n-type conducting polymer based on poly(isothianaphthene)*, Macromolecules **34**, 1810–1816 (2001)
[35] A. Cravino, M.A. Loi, M.C. Scharber, C. Winder, H. Neugebauer, P. Denk, H. Meng, Y. Chen, F. Wudl, N.S. Sariciftci, *Spectroscopic properties of PEDOTEHIITN, a novel soluble low band-gap conjugated polymer*, Synth. Met. **137**, 1435–1436 (2003)
[36] G. Sonmez, H. Meng, F. Wudl, *Very stable low band gap polymer for charge storage purposes and near-infrared applications*, Chem. Mater. **15**, 4923–4929 (2003)
[37] A. Kumar, Z. Buyukmumcu, G.A. Sotzing, *Poly(thieno[3,4-b]furan). A new low band gap conjugated polymer*, Macromolecules **39**, 2723–2725 (2006)
[38] B. Lee, V. Seshadri, G.A. Sotzing, *Poly(thieno[3,4-b]thiophene)-poly(styrene sulfonate): A low band gap, water dispersible conjugated polymer*, Langmuir **25**, 10797–10802 (2005)
[39] B. Lee, V. Seshadri, G.A. Sotzing, *Water dispersible low band gap conductive polymer based on thieno[3,4-b]thiophene*, Synth. Met. **152**, 177–180 (2005)
[40] M. Pomerantz, X. Gu, S.X. Zhang, *Poly(2-decylthieno[3,4-b]thiophene-4,6-diyl). A new low band gap conducting polymer*, Macromolecules **34**, 1817–1822 (2001)

[41] K. Lee and G.A. Sotzing, *Poly(thieno[3,4-b]thiophene). A new stable low band gap conducting polymer*, Macromolecules **34**, 5746–5747 (2001)
[42] V.S. Mylnikov, M. Biswas, A. Mukherjee, *Advances in polymers science 115: Photoconducting polymers/Metal-containing polymers*, Springer-Verlag, 132 pp. (1994)
[43] A.V. Patsis and D.A. Seanor (ed.), *Photoconductivity in polymers, an interdisciplinary approach*, Technomic Publishing, 377 pp. (1976)
[44] C.L. Braun, *Electric field assisted dissociation of charge transfer states as a mechanism of photocarrier production*, J. Chem. Phys. **80**, 4157–4161 (1984)
[45] N.C. Greenham, X. Peng, A.P. Alivisatos, *Charge separation and transport in conjugated-polymer/semiconductor-nanocrystal composites studied by photoluminescence quenching and photoconductivity*, Phys. Rev. B **54**, 17628–17637 (1996)
[46] M. Fox, *Oxford master series in condensed matter physics: Optical properties of solids*, Oxford University Press, 305 pp. (2001)
[47] D.V. Talapin, S.K. Poznyak, N.P. Gaponik, A.L. Rogach, A. Eychmüller, *Synthesis of surface-modified colloidal semiconductor nanocrystals and study of photoinduced charge separation and transport in nanocrystal-polymer composites*, Physica E **14**, 237–241 (2002)
[48] J. Joo, H.B. Na, T. Yu, J.H. Yu, Y.W. Kim, F. Wu, J.Z. Zhang, T. Hyeon, *Generalized and facile synthesis of semiconducting metal sulfide nanocrystals*, J. Am. Chem. Soc. **125**, 11100–11105 (2003)
[49] M.A. Hines and G.D. Scholes, *Colloidal PbS nanocrystals with size-tunable near-infrared emission: observation of post-synthesis self-narrowing of the particle size distribution*, Adv. Mater. **15**, 1844–1849 (2003)
[50] C.B. Murray, S. Sun, W. Gaschler, H. Doyle, T.A. Betley, C.R. Kagan, *Colloidal synthesis of nanocrystals and nanocrystal superlattices*, IBM J. Res & Dev. **45**, 47–56 (2001)
[51] W.W. Yu, J.C. Falkner, B.S. Shih, V.L. Colvin, *Preparation and characterization of monodisperse PbSe semiconductor nanocrystals in a noncoordinating solvent*, Chem. Mater. **16**, 3318–3322 (2004)
[52] D. Qi, M. Fischbein, M. Drndic, S. Selmic, *Efficient polymer-nanocrystal quantum-dot photodetectors*, Appl. Phys. Lett. **86**, 93103–93105 (2005)
[53] T.-W.F. Chang, S. Musikhin, L. Bakueva, L. Levina, M.A. Hines, P.W. Cyr, E.H. Sargent, *Efficient excitation transfer from polymer to nanocrystals*, Appl. Phys. Lett. **21**, 4295–4297 (2004)
[54] K. Roy Choudhury, Y. Sahoo, T.Y. Ohulchansky, P.N. Prasad, *Efficient photoconductive devices at infrared wavelengths using quantum dot-polymer nanocomposites*, Appl. Phys. Lett. **87**, 73110–73112 (2005)
[55] L. Bakueva, S. Musikhin, M.A. Hines, T.-W.F. Chang, M. Tzolov, G.D. Scholes, E.H. Sargent, *Size-tunable infrared (1000–1600 nm) electroluminescence from PbS quantum-dot nanocrystals in a semiconducting polymer*, Appl. Phys. Lett. **82**, 2895–2897 (2003)
[56] A. Watt, E. Thomsen, P. Meredith, H. Rubinsztein-Dunlop, *A new approach to the synthesis of conjugated polymer-nanocrystal composites for heterojunction optoelectronics*, Chem. Commun. **2004**, 2334–2335 (2004)
[57] A.A.R. Watt, H. Rubinsztein-Dunlop, P. Meredith, *A new approach to the synthesis of nanocrystal conjugated polymer composites*, Synth. Met. **154**, 57–60 (2005)
[58] A. Watt, H. Rubinsztein-Dunlop, P. Meredith, *Growing semiconductor nanocrystals directly in a conducting polymer*, Mater. Lett. **59**, 3033–3036 (2005)
[59] J.H. Warner and A.A.R. Watt, *Monodisperse PbS nanocrystals synthesized in a conducting polymer*, Mater. Lett. **60**, 2375–2378 (2006)
[60] S.A. McDonald, P.W. Cyr, L. Levina, E.H. Sargent, *Photoconductivity from PbS-nanocrystal/semiconducting polymer composites for solution-processible, quantum-size tunable infrared photodetectors*, Appl. Phys. Lett. **85**, 2089–2091 (2004)
[61] K. Roy Choudhury, Y. Sahoo, S. Jang, P. Prasad, *Efficient photosensitization and high optical gain in a novel quantum-dot-sensitized hybrid photorefractive nanocomposite at a telecommunications wavelength*, Adv. Funct. Mater. **15**, 751–756 (2005)
[62] K. Roy Choudhury, Y. Sahoo, P. Prasad, *Hybrid quantum-dot-polymer nanocomposites for infrared at an optical communication wavelength*, Adv. Mater. **17**, 2877–2881 (2005)
[63] J.S. Steckel, S. Coe-Sullivan, V. Bulovic, M.G. Bawendi, *1.3 μm to 1.55 μm tunable electroluminescence from PbSe quantum dots embedded within an organic device*, Adv. Mater. **15**, 1862–1866 (2003)
[64] G. Konstantatos, I. Howard, A. Fischer, S. Hoogland, J. Clifford, E. Klem, L. Levina, E.H. Sargent, *Ultrasensitive solution-cast quantum dot photodetectors*, Nature **442**, 180–183 (2006)
[65] H. Kim, K. Cho, H. Song, B. Min, J.-S. Lee, G.-T. Kim, S. Kim, *Photocurrent mechanism in a hybrid system of 1-thioglycerol-capped HgTe nanoparticles*, Appl. Phys. Lett. **83**, 4619–4621 (2003)
[66] H. Kim, K. Cho, B. Park, J.-H. Kim, J.W. Lee, S. Kim, T. Noh, E. Jang, *Optoelectronic characteristics of close-packed HgTe nanoparticles in the infrared range*, Solid State Commun. **137**, 315–319 (2006)
[67] M. Böberl, M.V. Kovalenko, S. Gamerith, E. List, W. Heiss, *Inkjet-printed nanocrystal photodetectors operating up to 3 μm wavelengths*, (submitted)